Ionic liquid-containing coordination polymer: solvent-free synthesis, incongruent melting, and glass formation

Mochida, Tomoyuki ; Qiu, Yi ; Funasako, Yusuke ; Inokuchi, Makoto ; Noguchi, Mariko ; Fujimori, Hiroki ; Furushima, Yoshitomo

(Citation)
Chemical Communications,58(47):6725-6728

(Issue Date)
2022-06-14

(Resource Type)
journal article

(Version)
Accepted Manuscript

COMMUNICATION

Ionic Liquid-Containing Coordination Polymer: Solvent-Free Synthesis, Incongruent Melting, and Glass Formation†

Received 00th January 20xx,
Accepted 00th January 20xx

DOI: 10.1039/x0xx00000x

Tomoyuki Mochida,[*ab] Yi Qiu,[a] Yusuke Funasako,[cd] Makoto Inokuchi,[c] Mariko Noguchi,[e] Hiroki Fujimori[e] and Yoshitomo Furushima[f]

An ionic-liquid-containing 2D coordination polymer was synthesized via a solvent-free reaction. The material exhibited incongruent melting at 112 °C, forming a solid–liquid mixture; further heating to 240 °C led to complete melting. Upon cooling, the melt transformed into a solid–liquid mixture, from which the coordination polymer was gradually recovered at ambient temperature. Rapid cooling (> 200 °C s^{-1}) of the melt resulted in complete vitrification at −28 °C.

A large number of coordination polymers (CPs), including metal-organic frameworks (MOFs), have been developed in the last few decades, prompted by interest in their useful properties such as gas absorption and catalytic activities. Most CPs decompose when heated instead of melting; however, several CPs that exhibit melting behavior have been recently reported.[1–8] Such materials have attracted significant attention due to their glass-forming properties, phase transformations, and processability, which enable the modification of structural properties and ion transport through hybridization, doping, and defect control. Previously, we reported the uncommon melting behavior of CPs [cation][MX_2] (M = alkali metal ions; X = polycyano anions) containing organometallic cations such as ferrocene.[9] These CPs exhibited incongruent melting, i.e., they produced a solid–liquid mixture of disproportionation products upon melting. However, these phenomenon could not be investigated in detail because of their high melting points and decomposition tendency. The melting behavior and glass formation of structurally related CP [cation][M(dicyanamide)$_3$] has been reported recently.[10] Herein, we investigated the incongruent melting and thermal behavior of a 2D CP [Emim][K(TCM)$_2$] (**1**; TCM = tricyanomethanide). The Emim cation is a representative component of ionic liquids[11] and it is thermally more robust than organometallic cations.

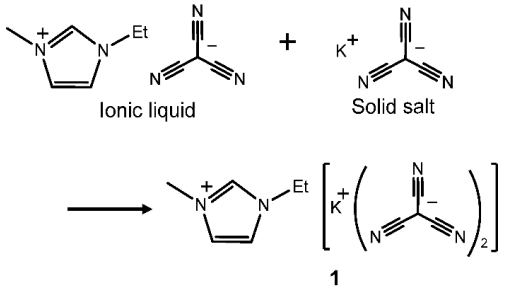

Fig. 1. Formation of **1** from [Emim][TCM] and K[TCM].

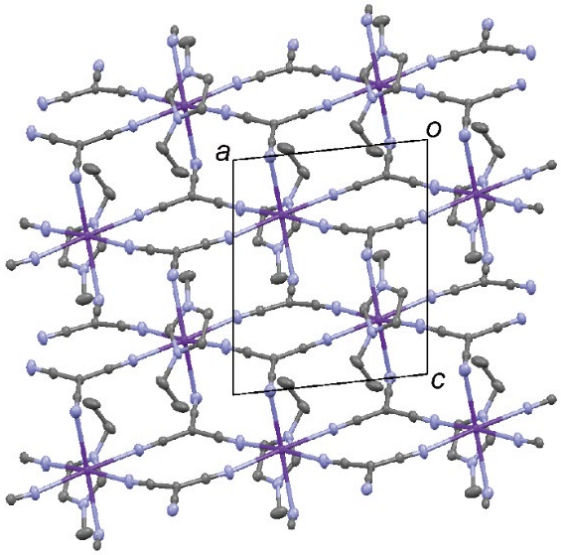

Fig. 2. Packing diagram of **1** (−173 °C) projected perpendicular to the 2-D framework (*b*-axis projection).

[a] *Department of Chemistry, Graduate School of Science, Kobe University, 1-1 Rokkodai, Nada, Kobe, Hyogo 657-8501, Japan. E-mail: tmochida@platinum.kobe-u.ac.jp*
[b] *Research Center for Membrane and Film Technology, Kobe University, 1-1 Rokkodai, Nada, Kobe, Hyogo 657-8501, Japan*
[c] *Department of Applied Chemistry, Faculty of Engineering, Sanyo-Onoda City University, 1-1-1, Daigakudori, Sanyo-Onoda, Yamaguchi 756-0884, Japan*
[d] *Department of Applied Chemistry and Biochemistry, National Institute of Technology, Wakayama College, 77 Noshima, Nada, Gobo, Wakayama, 644-0023, Japan*
[e] *Department of Chemistry, College of Humanities and Sciences, Nihon University, 3-25-40 Sakurajosui, Setagaya-ku, Tokyo 156-8550, Japan*
[f] *Materials Characterization Laboratories, Toray Research Center Inc., 3-7, Sonoyama 3-chome, Otsu, Shiga 520-8567, Japan*

†Electronic supplementary information (ESI) available: Experimental details, Crystallographic parameters, PXRD patterns, Raman spectra, Photographs, TG traces, and Video. CCDC 1869226 (**1**, −173 °C) and 2169840 (**1**, 20 °C). For ESI and crystallographic data in CIF or other electronic format see DOI: https://doi.org/10.1039/0000000

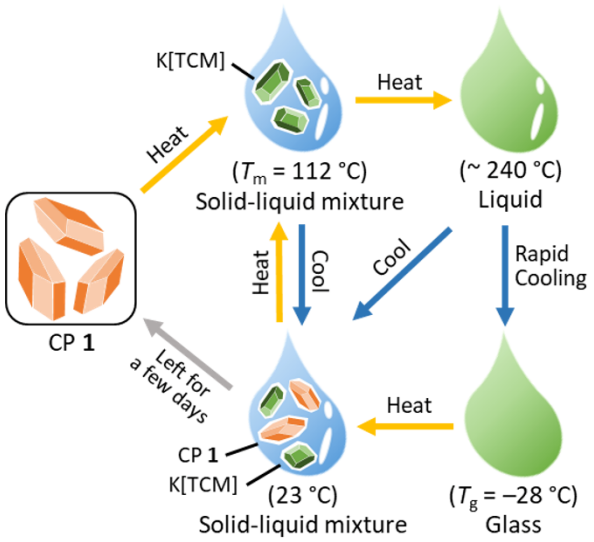

Fig. 3. Schematic of the phase behavior of **1**.

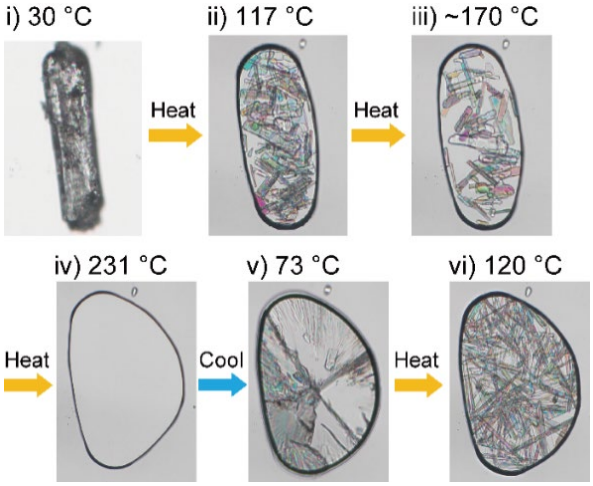

Fig. 4. POM images of **1** at different temperatures (heating and cooling rates of 20 °C min^{-1}): (i) crystalline state, (ii) after incongruent melting, (iii) dissolution of crystals, (iv) complete melting, (v) solidification (formation of solid–liquid mixture) upon cooling the liquid, and (vi) after incongruent melting upon reheating the solid.

CP **1** was prepared by the solvent-free reaction of an ionic liquid [Emim][TCM] with K[TCM] (**Fig. 1**). The mixture was ground with a mortar and pestle for 15 min at ambient temperature, upon which it gradually turned from a paste to the solid CP **1**. Alternatively, single crystals of **1** were grown by recrystallization of the mixture from EtOH–Et_2O. The solvent-free reaction product and the single crystals had identical structures as confirmed by powder X-ray diffraction (PXRD) measurements (**Fig. S1**, ESI†). X-ray crystal structure determination of **1** at −173 °C revealed that the complex, crystallized in space group *P*-1, exhibited an anionic 2-D CP framework composed of $[K(TCM)_2]^-_n$ (**Fig. 2**). The potassium ion has a six-coordinated octahedral coordination environment. The imidazolium cations are located between the anionic 2-D frameworks, resulting in a layered structure. The crystal structure at 20 °C was the same except that the ethyl substituent in the cation exhibited two-fold disorder (**Fig. S2**, ESI†).

The melting behavior of **1** was investigated by polarized microscopy (POM). The observed phase behavior of **1** is schematically summarized in **Fig. 3**. Upon heating, **1** exhibited melting at approximately 110 °C to produce a heterogeneous solid–liquid mixture (**Fig. 4, i–ii**). The melting was accompanied by the immediate growth and deposition of microcrystals, which upon further heating to ~240 °C, gradually dissolved to form a uniform liquid (**Fig. 4, iii–iv**). When cooled, the liquid solidified at approximately 75 °C to form a solid–liquid mixture (**Fig. 4, v**). When reheated, the solid again exhibited incongruent melting (**Fig. 4, vi**). The melting and solidification process is shown in **Video S1** in the ESI†.

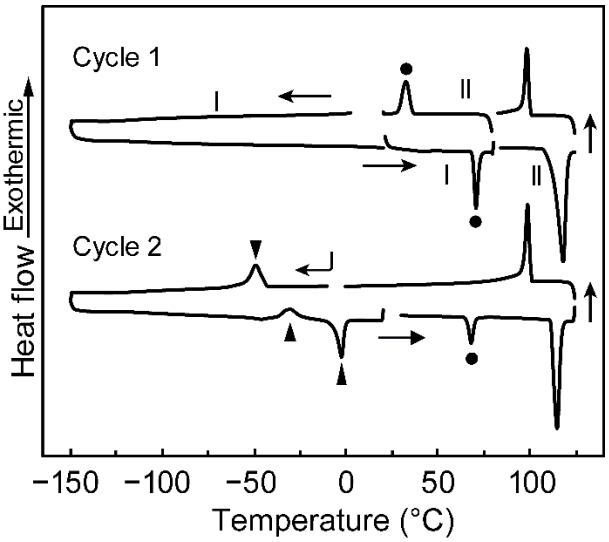

Fig. 6. DSC traces of **1** measured up to 125 °C. The solid triangles indicate the solidification and melting of the ionic liquid component. The solid circles indicate the solid phase transition between phase I and II. The reversibility of the phase transition was investigated in the range 20–80 °C in the first cycle.

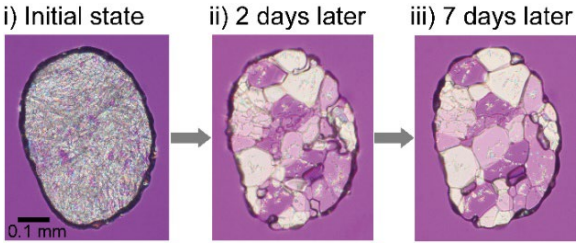

Fig. 6. POM images of the sample formed by cooling the melt of **1** to 23 °C: (i) immediately after cooling, and after leaving the sample for (ii) 2 days and (iii) 7 days at 23 °C. A heterogeneous mixture of **1**, K[TCM], and [Emim][TCM] is formed upon cooling, but it gradually transformed into **1**, forming large crystalline domains.

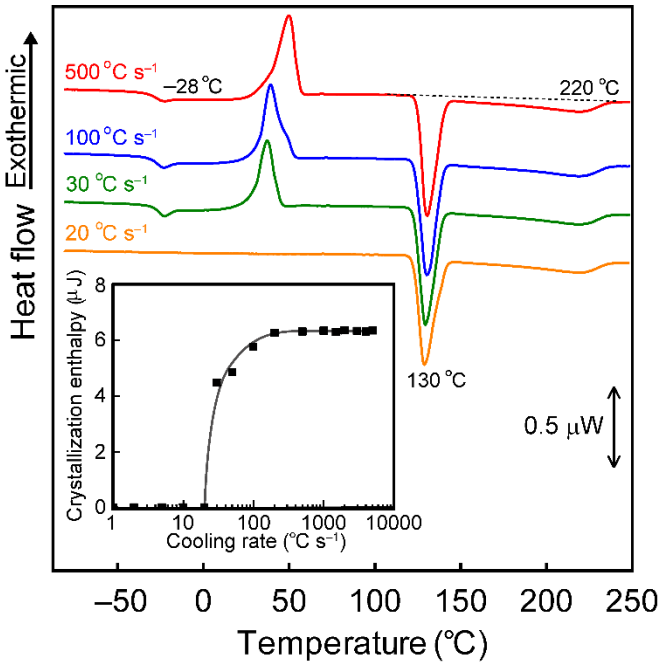

Fig. 7. FSC traces of the sample cooled from the melt at various cooling rates (20, 30, 100, and 500 °C s^{-1}), recorded upon heating at 1000 °C s^{-1}. When cooled at 20°C, crystallization occurs during cooling, hence only a melting peak is observed. However, when cooled at higher rates, glass transition, cold crystallization, and melting are successively observed because of vitrification upon cooling. The inset shows the enthalpies of cold crystallization observed at approximately 50 °C, plotted as a function of cooling rate.

The mechanism of the incongruent melting process was then investigated. The microcrystals formed upon incongruent melting consisted of K[TCM], which was confirmed via Raman microscopy and PXRD (**Figs. S3** and **S4**, ESI†). Raman spectra of the solid–liquid mixture at 120 °C showed the CN stretching peaks of K[TCM] (2173 and 2225 cm^{-1})[12] and [Emim][TCM] (2165 and 2211 cm^{-1})[13], indicating that the formation of the solid–liquid mixture corresponds to the deposition of K[TCM] crystals owing to their low solubility in the ionic liquid phase at the melting point of **1**. Interestingly, when the solid–liquid mixture formed at T_m (112 °C) was maintained at 120 °C for several hours, the crystal size increased (**Fig. S6**, ESI†), which was ascribed to Ostwald ripening owing to the dissolution equilibrium and high crystallinity of K[TCM].

Differential scanning calorimetry (DSC) was performed to understand the thermodynamic features of the melting behavior of **1** (**Fig. 5**). Upon heating, **1** exhibited a solid phase transition at 68.9 °C (ΔH = 5.1 kJ mol^{-1}) and incongruent melting at T_m = 112 °C (onset 105 °C, peak-top 118 °C, ΔH_m = 20.6 kJ mol^{-1}). The observed melting enthalpy is the sum of the enthalpies of the melting of **1** and partial deposition of K[TCM]. Upon cooling the mixture from 125 °C, the CP crystallized at ~90 °C, producing a mixture of **1**, K[TCM], and liquid [Emim][TCM]; the liquid phase may contain some dissolved K[TCM]. The crystallization and melting of [Emim][TCM] were observed in the second cycle at approximately −40 and −7 °C, respectively (**Fig. 5**, bottom). Notably, the latter temperature is consistent with the previously reported value of T_m = −11 °C for [Emim][TCM].[14]

In the second cycle, the CP component formed in the first cycle exhibited incongruent melting at 110 °C. However, the enthalpy change ($\Delta H_m'$ = 9.4 kJ mol^{-1}) was about half that of the first cycle, indicating that the amount of **1** crystallized in the first cycle was about half the initial amount, whereas the other half existed as a mixture of K[TCM] deposited at T_m (110 °C) and liquid [Emim][TCM]. The molar ratio of these three components (~1:1:1) was independent of the cooling rate (5–30 °C min^{-1}). In subsequent cycles, the melting and solidification behavior was similar to that observed in the second cycle.

Subsequently, the thermal behavior above T_m was investigated. Raising the temperature above T_m resulted in the gradual dissolution of K[TCM] into the liquid phase, which was observed as a very broad peak in the DSC trace (peak-top 220 °C, ΔH = 14 kJ mol^{-1}; see below. Upon cooling the liquid, solidification occurred at ~90 °C, producing a mixture of **1**, K[TCM], and liquid [Emim][TCM] in a similar ratio to that formed upon cooling the solid–liquid mixture formed at T_m. Thus, the liquid does not crystallize into a pure CP or exhibit vitrification when cooled from the liquid state under standard cooling conditions. Interestingly, when left at ambient temperature (23 °C), the thus-formed heterogeneous mixture spontaneously transformed into crystalline **1** within several days. This transformation was visually observed by POM as the gradual formation of large crystalline domains of **1** (**Fig. 6**). The complete recovery of **1** was confirmed by Raman and DSC measurements. These processes are also included in **Fig. 3**. This self-recovery-like phenomenon is unconventional in CPs, but it is thermodynamically reasonable considering the solvent-free formation of **1** from [Emim][TCM] and K[TCM], as demonstrated above.

Furthermore, the thermal stability of **1** was evaluated via thermogravimetric (TG) analysis. The weight loss temperature (−5 wt%) of **1** was 352 °C. However, slight decomposition occurred when **1** was maintained at ≥ 250 °C for more than a few minutes, which was observed in the DSC trace as a small decrease in ΔH_m.

As discussed above, the material gives a heterogeneous mixture when cooled from the liquid state under standard cooling conditions. However, rapid cooling from the melt resulted in glass formation (**Fig. 3**), as revealed by fast scanning calorimetry (FSC) measurements. A single crystal of **1** was heated to 250 °C and then the melt was cooled to −80 °C at rates of 20–5000 °C s^{-1}. The FSC traces were then recorded upon heating the obtained samples at 1000 °C s^{-1} (**Fig. 7**). Glass formation was observed when the cooling rate was ≥ 30 °C s^{-1}. Upon heating the glass, the glass transition was observed at −28 °C, followed by crystallization at ~50 °C, and incongruent melting at ~130 °C (**Fig. 7**; 30, 100, and 500 °C s^{-1} data**)**. A very broad peak with a peak-top temperature of 220 °C was observed, which corresponds to the dissolution of K[TCM] into the liquid phase. The observed glass transition temperature is reasonable because its ratio to the melting point (T_m = 112 °C) in Kelvin is 0.64, which is close to the empirical value for molecular liquids (T_g/T_m = 2/3).[15] In contrast, the sample prepared by cooling the melt at 20 °C s^{-1} crystallized; hence, neither glass transition nor cold crystallization was observed in the FSC trace during heating (**Fig. 7**; 20 °C s^{-1} data).

The degree of partial crystallization that occurred when cooling the melt can be estimated from the enthalpy of cold crystallization observed at approximately 50 °C in the FSA trace. The enthalpy values at various cooling rates are shown in the inset of **Fig. 7**. The value increased as the cooling rate increased from 30 to 100 °C s^{-1}, indicating incomplete glass formation, whereas complete vitrification was observed at faster cooling rates (≥ 200 °C s^{-1}).

Other typical 2-D or 3-D melting CPs such as $[Zn(H_2PO_4)_2(triazole)_2]$ (T_m = 184 °C)[4] and [Zn(imidazolate)$_4$] (ZIF-4; T_m = 593 °C)[5] form glasses by melt quenching under standard cooling conditions. However, the current CP (T_m = 112 °C) required a much faster cooling rate for glass formation. This behavior is ascribed to its low melting point and low viscosity in the liquid state, which are the consequences of using the ionic liquid component.

In summary, we synthesized a CP that exhibits incongruent melting, using an imidazolium ionic liquid and a solid salt, both containing TCM as a common ion. This hybridization method is a unique design strategy for CPs with low melting points and can be extended to other CPs.[9] Notably, the CP could be prepared by solvent-free reaction and exhibited self-recovery from the ionic liquid/metal salt mixture, which are due to the ionic liquid component. The application of ionic liquids is a useful approach to processable CPs. Indeed, some melting CPs are structurally related to ionic liquids[1,8] and ionic liquids incorporated into the pores of MOFs facilitates melting.[16] In this study, we investigated the details of the incongruent melting of the prepared CP. Although incongruent melting is rare in CPs,[9,17-20] we expect more such cases to be found as it is a common phenomenon in multicomponent solids such as alloys and minerals. This is the first report of the application of FSC to melting coordination polymers. Polymers and molecular materials typically undergo vitrification when the cooling rate is fast enough.[21] Therefore, coordination polymers that crystallize upon cooling should vitrify upon sufficient rapid cooling; their thermodynamics is of interest and will be a subject of future studies using FSC.

We thank Ryo Sumitani and Hironori Kimata (Kobe University) for their help with the experiments. This work was supported financially by KAKENHI (grant number 20K21210) from the Japan Society for the Promotion of Science (JSPS).

Author Contributions

T. Mochida: conceptualization, investigation, and writing. Y. Qiu: synthesis and XRD experiments. Y. Funasako and M. Inokuchi: Raman spectroscopy. M. Noguchi, H. Fujimori, and Y. Furushima: thermal analyses.

Conflicts of interest

There are no conflicts to declare.

Notes and references

1 T. D. Bennett and S. Horike, *Nat. Rev. Mater.*, 2018, **3**, 431–440.
2 N. Ma and S. Horike, *Chem. Rev.*, 2022, **122**, 4163–4203.
3 S. Horike, S.S. Nagarkar, T. Ogawa and S. Kitagawa, *Angew. Chem., Int. Ed.,* 2020, **59**, 6652–6664.
4 D. Umeyama, S. Horike, M. Inukai, T. Itakura and S. Kitagawa, *J. Am. Chem. Soc.*, 2015, **137**, 864–870.
5 T. D. Bennett, J. Tan, Y. Yue, E. Baxter, C. Ducati, N. J. Terrill, H. H. Yeung, Z. Zhou, W. Chen, S. Henke, A. K. Cheetham and G. N. Greaves, *Nat. Commun.*, 2015, **6**, 1–7.
6 L. Longley, S.M. Collins, C. Zhou, G. J. Smales, S. E. Norman, N. J. Brownbill, C. W. Ashling, P. A. Chater, R. Tovey, C. B. Schonlieb, T. F. Headen, N. J. Terrill, Y. Z. Yue, A. J. Smith, F. Blanc, D. A. Keen, P. A. Midgley and T. D. Bennett, *Nat. Commun.*, 2018, **9**, 2135.
7 K. Tanaka, Y. Tago, M. Kondo, Y. Watanabe, K. Nishio, T. Hitosugi and M. Moriya, *Nano Lett.*, 2020, **20**, 8200–8204.
8 M. Liu, R. D. McGillicuddy, H. Vuong, S. Tao, A. H. Slavney, M. I. Gonzalez, S. J. L. Billinge and J. A. Mason, *J. Am. Chem. Soc.*, 2021, **143**, 2801–2811.
9 H. Kimata and T. Mochida, *Chem. Eur. J.*, 2019, **25**, 10111–10117.
10 B. K. Shaw, A. R. Hughes, M. Ducamp, S. Moss, A. Debnath, A. F. Sapnik, M. F. Thorne, L. N. McHugh, A. Pugliese, D. S. Keeble, P. Chater, J. M. Bermudez-Garcia, X. Moya, S. K. Saha, D. A. Keen, F.-X. Coudert, F. Blanc and T. D. Bennett, *Nat. Chem.*, 2021, **13**, 778–785.
11 Kar, M.; Matuszek, K. and D. R. MacFarlane, Ionic Liquids. In *Kirk–Othmer Encyclopedia of Chemical Technology*; John Wiley & Sons, Inc., 2019.
12 A. Bernsdorf, H. Brand, R. Hellmann, M. Köckerling, A. Schulz, A. Villinger and K. Voss, *J. Am. Chem. Soc.,* 2009, **131**, 8958–8970.
13 A. I. Labropoulos, G. E. Romanos, E. Kouvelos, P. Falaras, V. Likodimos, M. Francisco, M. C. Kroon, B. Iliev, G. Adamova and T. J. S. Schubert, *J. Phys. Chem. C,* 2013, **117**, 10114−10127.
14 Y. Yoshida, K. Muroi, A. Otsuka, G. Saito, M. Takahashi and T. Yoko, *Inorg. Chem.*, 2004, **43**, 1458–1462.
15 D. Turnbull and M. H. Cohen, Crystallization Kinetics and Glass Formation. In *Modern Aspects of the Vitreous State*; J. D. MacKenzie, ed., Butterworth, London, 1960.
16 V. Nozari, C. Calahoo, J. M. Tuffnell, D. A. Keen, T. D. Bennett and L. Wondraczek, *Nat. Commun.*, 2021, **12**, 5703.
17 D. V. Soldatov and J. A. Ripmeester, *Chem. Mater.,* 2000, **12**, 1827–1839.
18 F. J. M. Casado, M. R. Riesco, I. da Silva, M. I. R. Yélamos, A. Labrador and J. A. R. Cheda, *Cryst. Growth Des.,* 2011, **11**, 759–767.
19 E. A. Ukraintseva, D. V. Soldatov, L. N. Zelenina, P. E. Plyusnin and A. G. Ogienko, *Russ. J. Phys. Chem.*, 2006, **80**, 1920–1924.
20 V. Nozari, C. Calahoo, L. Longley, T. D. Bennett and L. Wondraczek, *J. Chem. Phys.*, 2020, **53**, 204501.
21 C. Schick, V. Mathot, Eds.; *Fast Scanning Calorimetry*; Springer, 2016.

TOC

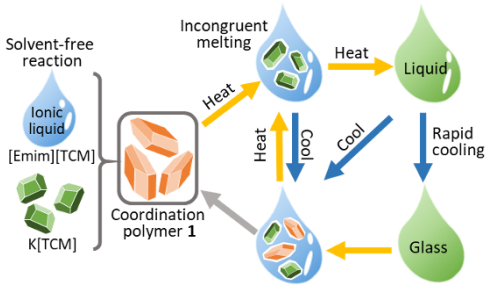

We prepared a 2-D coordination polymer that exhibits incongruent melting; the phase behaviour was investigated in detail.

Supporting Information

Tomoyuki Mochida,*[ab] Yi Qiu,[a] Yusuke Funasako,[cd] Makoto Inokuchi,[c] Mariko Noguchi,[e] Hiroki Fujimori,[e] Yoshitomo Furushima[f]

[a]*Department of Chemistry, Graduate School of Science, Kobe University, 1-1 Rokkodai, Nada, Kobe, Hyogo 657-8501, Japan. E-mail: tmochida@platinum.kobe-u.ac.jp*

[b]*Research Center for Membrane and Film Technology, Kobe University, 1-1 Rokkodai, Nada, Kobe, Hyogo 657-8501, Japan*

[c]*Department of Applied Chemistry, Faculty of Engineering, Sanyo-Onoda City University, 1-1-1, Daigakudori, Sanyo-Onoda, Yamaguchi 756-0884, Japan*

[d]*Department of Applied Chemistry and Biochemistry, National Institute of Technology, Wakayama College, 77 Noshima, Nada, Gobo, Wakayama, 644-0023, Japan*

[e]*Department of Chemistry, College of Humanities and Sciences, Nihon University, 3-25-40 Sakurajosui, Setagaya-ku, Tokyo 156-8550, Japan*

[f]*Materials Characterization Laboratories, Toray Research Center Inc., 3-7, Sonoyama 3-chome, Otsu, Shiga 520-8567, Japan*

Contents

Experimental

General. DSC was performed using a TA Instrument Q100 differential scanning calorimeter with sweep rates of 10–30 °C min^{-1} under a nitrogen atmosphere. TG analyses were performed at 10 °C min^{-1} under a nitrogen atmosphere using a Rigaku TG8120 analyzer. Infrared (IR) spectra were recorded via attenuated total reflectance (ATR diamond) using a Thermo Scientific Nicolet iS 5 FT-IR spectrometer. Raman spectra were measured using a Renishaw Ramascope System 1000 spectrometer (λ_{ex} = 780 nm). PXRD measurements were performed using Bruker APEX II Ultra and Rigaku Smartlab diffractometers. FSC measurements were conducted using a Mettler Toledo Flash DSC 1 instrument under a nitrogen atmosphere. A single crystal of **1** was heated to 250 °C at 100 °C min^{-1}, maintained at this temperature for 5 s, and then cooled to −80 °C at various cooling rates (20–500 °C s^{-1}). Subsequently, FSC traces were recorded upon heating the sample to 250 °C at 1000 °C s^{-1}. The measurements at various cooling rates were conducted using the same sample.

Synthesis of 1. The recrystallization of a mixture of [Emim][TCM][S1] (16.8 mg, 0.08 mmol) and K[TCM] (11 mg, 0.08 mmol) from Et_2O–EtOH yielded the desired complex as colorless needle crystals, which were collected by filtration and dried under vacuum (9.7 mg, 35%). Grinding equimolar amounts of [Emim][TCM] and K[TCM] using a mortar and pestle also produced **1** quantitatively. Anal. Calcd. for $C_{14}H_{11}N_8K$: C, 50.90; H, 3.36; N, 33.92. Found: C, 50.90; H, 2.99; N, 33.51. IR (cm^{-1}): 2160 (CN), 1572, 1236, 1167, 840, 746, 702, 621, 563, 526. The material was not hygroscopic and completely stable under atmospheric condition.

X-ray structure determination. The X-ray diffraction data were collected on a Bruker APEX II Ultra CCD diffractometer at −173 °C and 20 °C with MoKα radiation (λ = 0.71073 Å). All calculations were performed using SHELXTL.[S2] The crystallographic parameters are shown in **Table S1**. CSD number: CCDC 1869226 (data at −173 °C) and 2169840 (data at 20 °C).

References

[S1] Y. Yoshida, K. Muroi, A. Otsuka, G. Saito, M. Takahashi, T. Yoko, *Inorg. Chem.* 2004, **43**, 1458–1462.

[S2] G. M. Sheldrick, *Acta Crystallogr*. 2008, **C64**, 112–122.

[S3] J. R. Witt, D. Britton, *Acta Cryst.* 1971, **27**, 1835–1836.

Table S1. Crystallographic parameters of **1** at −173 and 20 °C

	−173 °C	20 °C
Empirical formula	$C_{14}H_{11}N_8K$	
Formula weight	330.41	
Crystal system	Triclinic	Triclinic
Space group	*P*-1	*P*-1
a (Å)	8.5703(8)	8.6092(12)
b (Å)	9.7142(10)	9.8641(14)
c (Å)	10.2374(10)	10.4829(15)
α (°)	83.6370(10)	83.222(2)
β (°)	83.0040(10)	82.672(2)
γ (°)	81.1040(10)	81.215(2)
V (Å^3)	832.09(14)	868.2(2)
Z	2	2
ρ_{calcd} (g cm^{-3})	1.319	1.264
F (000)	340	340
Reflns collected	4019	4433
Independent reflns	2878	3222
Parameters	210	230
Temperature (K)	100	293
R_1[a], R_w[b] ($I > 2\sigma$)	0.0336, 0.0878	0.0481, 0.1287
R_1[a], R_w[b] (all data)	0.0342, 0.0883	0.0557, 0.1357
Goodness of fit	1.076	1.045
$\Delta\rho_{max,min}$ [e Å^{-3}]	0.376, –0.380	0.334, −0.22

[a]$R_1 = \Sigma||F_o| - |F_c|| / \Sigma|F_o|$; [b]$R_w = [\Sigma w (F_o^2 - F_c^2)^2/\Sigma w(F_o^2)^2]^{1/2}$.

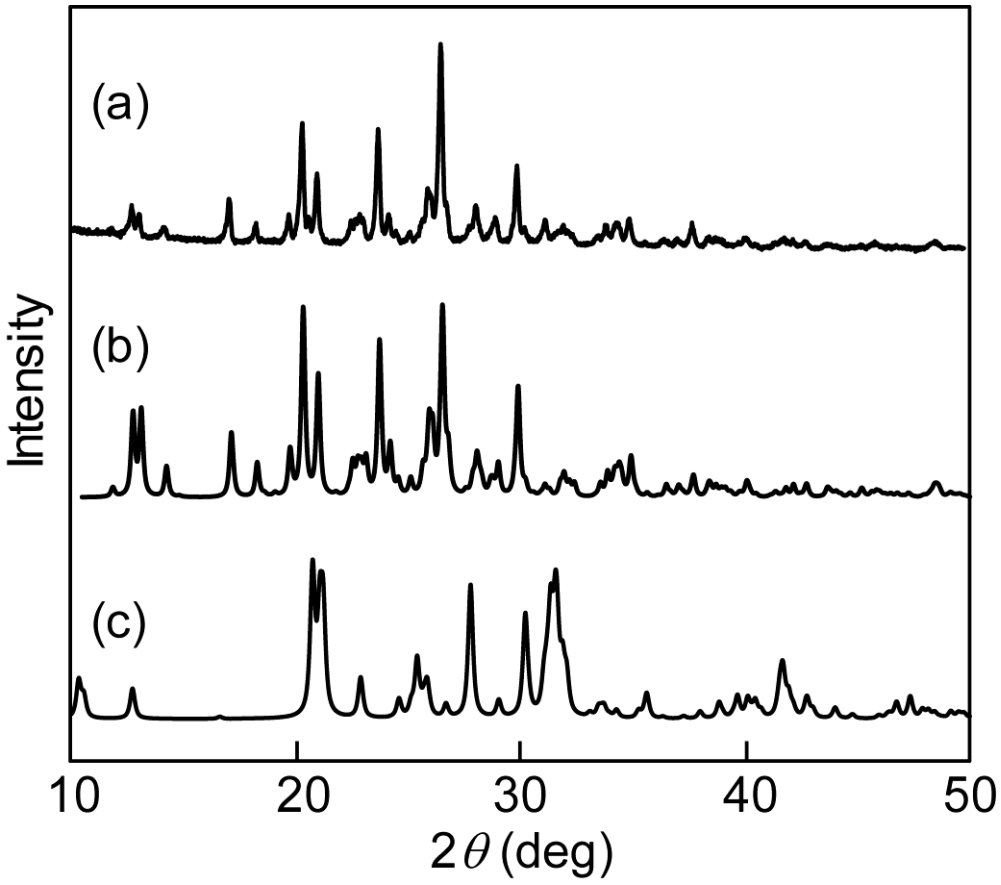

Fig. S1. PXRD patterns of (a) **1** formed by grinding [Emim][TCM] and K[TCM] for 1 h at 22 °C, (b) **1** simulated from the single crystal data at 20 °C, and (c) K[TCM] simulated from the single crystal data.[S3]

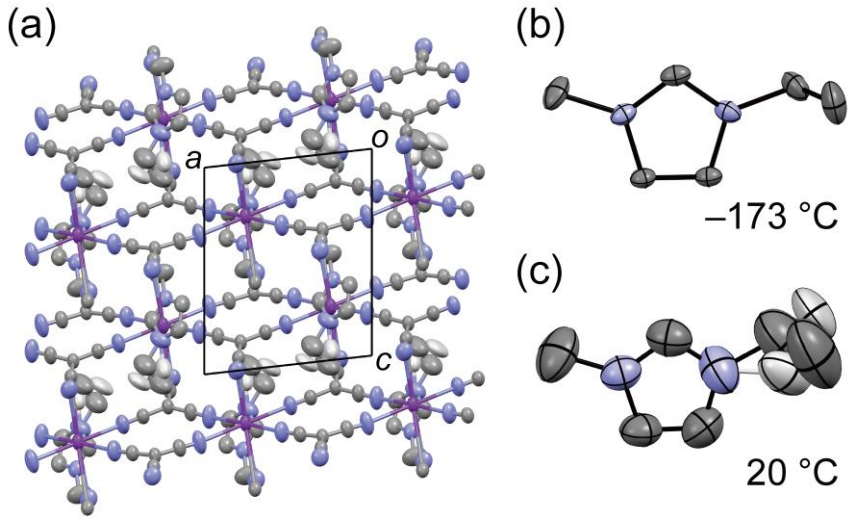

Fig. S2. (a) Packing diagram of **1** determined at 20 °C. (b) ORTEP drawings of the molecular structures of the cations determined at −173 °C (top) and 20 °C (bottom, occupancy ratio = 0.7:0.3).

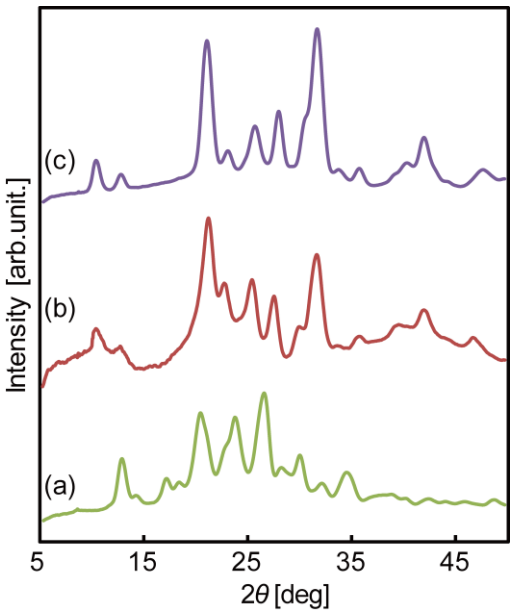

Fig. S3. PXRD patterns of (a) **1** at 22 °C, (b) **1** after incongruent melting at 150 °C, and (c) K[TCM] at 22 °C (Cu*K*α radiation).

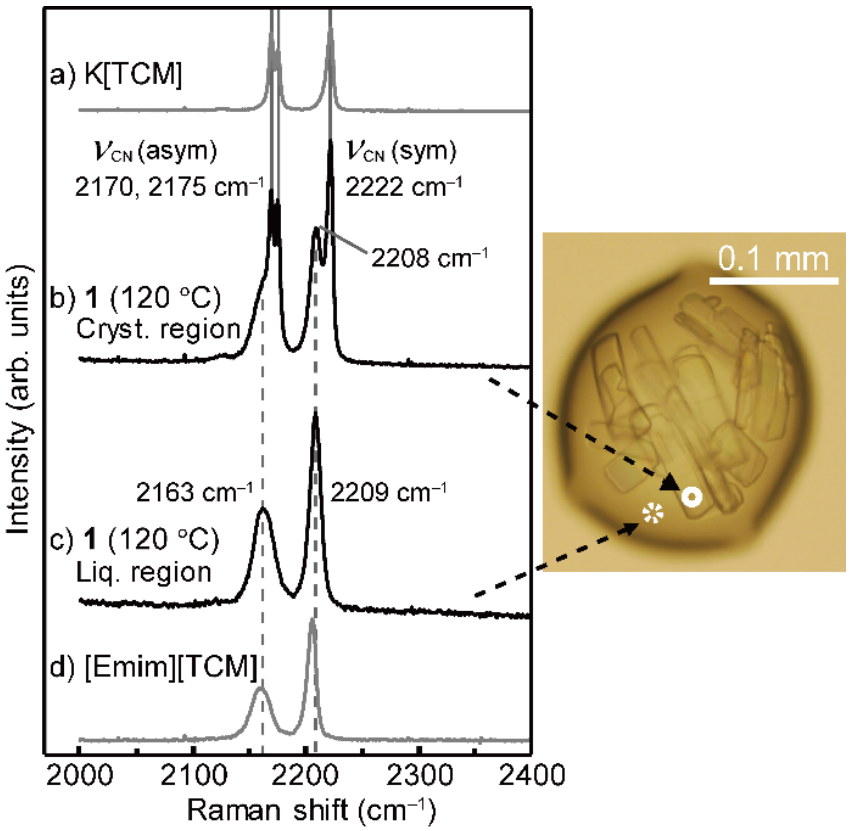

Fig. S4. Raman spectra of (a) K[TCM] (20 °C), (b) **1** after incongruent melting (120 °C, solid-rich region), (c) **1** after incongruent melting (120 °C, liquid region), and (d) [Emim][TCM] (20 °C). In the photograph of the sample at 120 °C shown on the right, the circles represent the regions for which the Raman spectra were recorded.

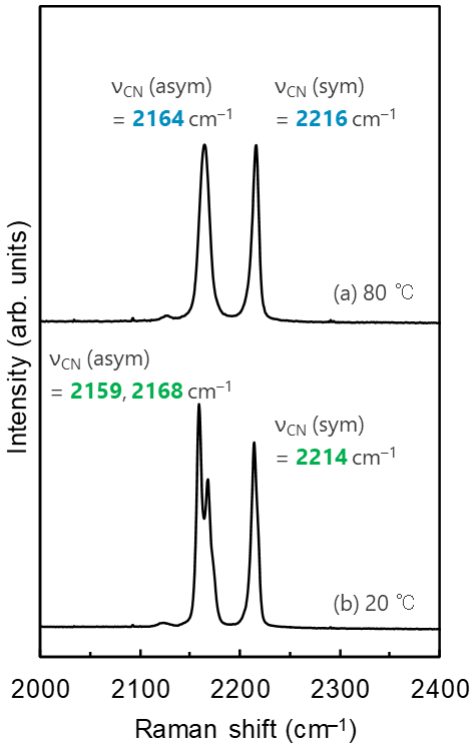

Fig. S5. Raman spectra of **1** measured at (a) 80 °C and (b) 20 °C.

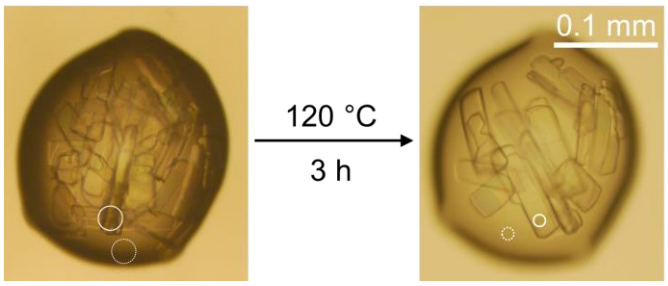

Fig. S6. Photographs of **1** taken at 120 °C after incongruent melting (left) and after standing at the same temperature for 3 h (right).